A study of hot pixel annealing in the Hubble Space Telescope Wide Field Camera 3 CCDs

Elizabeth J. Polidan[a], Augustyn Waczynski[a], Paul Marshall[b], Scott D. Johnson[a], Cheryl Marshall[c], Robert Reed[c], Randy A. Kimble[c], Gregory Delo[a], David Schlossberg[d], Anne Marie Russell[a], Terry Beck[d], Yiting Wen[e], John Yagelowich[c], Robert J. Hill[e]

[a]Global Science & Technology,NASA/Goddard Space Flight Center, Greenbelt,MD 20771 USA
[b]NASA Consultant, Brookneal, VA 24528 USA
[c]NASA/Goddard Space Flight Center, Greenbelt, MD 20771 USA
[d]Sigma, NASA/GSFC, Greenbelt, MD 20771 USA
[e]SSAI, NASA/GSFC, Greenbelt, MD 20771 USA

ABSTRACT

A Hubble Space Telescope Wide Field Camera 3 (WFC3) CCD detector was tested for radiation effects while operating at -83°C. The goal of the experiment was to evaluate the introduction and annealing rates of hot pixels and to assess the dynamics of that process. The device was irradiated while cold and warmed to +30°C for a 4 hour soak, then cooled back down to -83°C. Hot pixel populations were tracked during warm up and cool down. The results showed that the hot pixels begin to anneal around -40°C and the anneal process was largely completed before the detector reached +30°C. It was also found that, although a large fraction of the hot pixels dropped below the threshold, they remained warmer than the remaining population.

Keywords: detector, CCD, hot pixels, hot pixel annealing, radiation damage, WFC3, HST, e2v

1. INTRODUCTION

The space radiation environment degrades the performance of charge-coupled device (CCD) based instruments. Radiation damage to the CCD's silicon lattice results in a reduction of the charge transfer efficiency and an increased dark current generation in pixels where damage occurred. Excessive dark current renders these pixels useless for science applications. Effects of radiation damage have been observed in a number of instruments deployed in space, including instruments aboard the Hubble Space Telescope (HST).[1, 2] Radiation induced high dark current pixels (hot pixels) have been observed in all of the CCD based instruments. It was also observed that hot pixels largely anneal when exposed to room temperature. Annealing at such a low temperature was unexpected and not well understood. Different annealing rates were reported for different instruments and the cause of the difference was not obvious. It was expected that the annealing temperature was a significant factor.

The Wide Field Camera 3 (WFC3) project conducted an extensive study of the radiation damage to CCD and IR detectors.[3, 4] Flight like CCDs went through numerous passive radiation exposures to determine the change in charge transfer efficiency with fluence. A separate experiment was designed to study hot pixel behavior by exposing a flight like CCD to radiation under operating conditions to determine hot pixel introduction and annealing rates and to validate the project's planned hot pixel annealing procedure.

A first paper[5] reported hot pixel introduction and annealing rates resulting from 4 hour soaking at +30°C. The hot pixel population at -83°C was tracked through exposure to the proton beam and before and after the anneal step. The results validated WFC3's plan for a monthly anneal at +30°C. This paper attempts to evaluate the dynamics of hot pixel annealing as a function of temperature from the existing data.

Further author information: (Send correspondence to E.J.P.)
E.J.P.: E-mail: epolidan@cte.gsfc.nasa.gov, Telephone: 1 310 519 7488

2. EXPERIMENT

The test was performed in 4 different steps. The three initial steps were to simulate the WFC3 monthly anneal cycle in space; the fourth step was designed to verify dark current and hot pixel population changes after the instrument had spent half its lifetime in space. In the first through third steps the detector was exposed, while cold, to a fluence of $8.33 \times 10^7/\mathrm{cm}^2$ of 63.3 MeV protons per step. This simulated 1 month per step in the radiation environment of the WFC3 instrument on the HST.[6,7] After irradiation, the CCD was kept at the WFC3 operating temperature of -83°C and several dark exposures were taken to measure the number of hot pixels introduced. The device was then slowly warmed, stopping at -40°C, -20°C, -10°C, 0°C, +10°C, +20°C, and +30°C to take dark exposures. The CCD was then left to soak for 4 hours at +30°C. After the soak the device was cooled down to -83°C and a series of dark exposures was taken. Each of the first three irradiate/anneal steps simulated 3 separate months of the planned hot pixel mitigation strategy for WFC3.

The fourth step was similar to the first through third steps, except that the CCD was exposed to a fluence of $2.25 \times 10^9/\mathrm{cm}^2$ of 63.3 MeV protons, a dosage equivalent to 27 months in the WFC3 radiation environment. This brought the total exposure on the device to the equivalent of 2.5 years in the WFC3 environment. The test procedure is more thoroughly described in the previous paper on this subject.[5]

WFC3 is using a custom designed CCD43-62 from e2v (formerly EEV). The detector has a format of 2kx4k, a serial readout register placed on the longer side and two amplifiers, one on each end of the serial register. The CCD can be read using one or both amplifiers. The detector has a supplemental buried channel in both the parallel and serial registers for improved charge transfer efficiency at lower signal levels. It operates in IMO mode which suppresses surface states and significantly lowers dark current generation. Throughout this experiment the detector was run under WFC3 operating conditions with a readout speed of 50 kHz per channel and with each amplifier reading the corresponding half of the image.

The mean dark current in the detector operating in the IMO mode and at the instrument's operating temperature of -83°C is remarkably low, in the range of 0.1 e^-/px/hr before irradiation. At these levels accurate measurements are very difficult and the thermal component of dark current is often masked by other effects like charge release from trapping centers or baseline instability. Multiple exposures were necessary for random event rejection. As a compromise between available time at the accelerator and the precision of hot pixel determination, five exposures were taken at each temperature: two short bias frames and three dark exposures with exposure time varying with temperature. At -83°C the dark exposure had to be 1.5 hours long to produce meaningful results.

The detector used for this experiment was an engineering grade CCD with a small defect in the serial register which limited full well to approximately 40 ke^- for the left half of the image (read with the A amplifier). The data presented here are based on the right hand side of the image (B amplifier readout) as this side had a smaller number of saturated pixels.

3. ANALYSIS

The primary objective of the experiment was to determine hot pixel introduction and annealing rates for the WFC3 applications. A secondary goal was to study the hot pixel annealing process, a challenge due to certain limitations. The first was the limited understanding of the annealing process and lack of a theoretical model. Therefore a large temperature range was used to ensure that the onset temperature was caught.

The other challenge was the limitations in the experimental setup. Mean dark and hot pixel changes with radiation and temperature could not be fully compensated by gain and exposure time adjustment. As a result, the number of saturated hot pixels varies widely from one temperature step to another, and only a small fraction of the pixels is available for this analysis. During the experiment the detector was operated as it would be in the application: in slow readout mode. At warmer temperatures this readout time became comparable to, or even higher than, the exposure time and many of the hot pixels saturate and smear as they are shifted and read (figure 1(a)). The solution to the smear was to create a bias for each temperature using 1 second exposures. These biases contained the same saturated hot pixels and the same smearing. When the biases were subtracted from the dark exposures the streaking was removed. Figure 1(b) shows the fairly successful correction of a 10

(a) **(b)**

Figure 1. Side a is a 10 sec dark frame taken at +30°C and shows streaks due to saturation of the upper half of the frame. Side b shows how well this frame is corrected by subtracting a 1 sec dark.

second dark taken at +30°C. This blooming could not be fully corrected for which resulted in some degree of distortion in the dark current histogram, in particular on the low side of the distribution.

Two methods were tested to determine hot pixels: referencing the hot pixel threshold to the mean dark, and using a fixed threshold. As the mean dark was very low and was fluctuating (due to other factors), hot pixel estimates based on the mean were not reliable. The fixed threshold approach was chosen instead and it produced consistent results. Multiple threshold levels were used to better track the hot distribution. Using three 1.5 hour exposures at -83°C, which were taken immediately after irradiation, hot pixels were identified using three different thresholds: >40 e^-/px/hr, >80 e^-/px/hr, and >160 e^-/px/hr. Random events (such as cosmic ray hits or the decay of proton beam induced activity) were defined as signal greater than 40 e^-/px/hr present in one or two, but not three of the 1.5 hour exposures. These events were identified and removed. The defined set of hot pixels was then over plotted onto the dark histogram of the entire array (including "normal" pixels and hot pixels) at each temperature.

At temperatures warmer than -83°C annealed pixels were defined as hot pixels whose dark rate had decreased to less than 100x (or 200x) the mean dark rate. These levels were chosen because they correspond to the thresholds for the hot pixels identified at -83°C ($40e^-$ is approximately equal to 100x the mean dark current immediately after irradiation). The annealed pixels were plotted as a function of temperature to investigate the onset temperature of the anneal process.

4. RESULTS

Table 1 summarizes the introduction and annealing rates for each step in the experiment. Note that in the first step of the experiment, prior to, during, and after the first month radiation dose the ^{55}Fe actuator had slipped down into the dewar enough to expose the CCD. This was noticed during the initial quick look analysis immediately after this phase and was quickly corrected; all further data was not contaminated. As can be seen from the annealing rates for the different thresholds, the hotter pixels are more likely to anneal than the warm hot pixels.

The subsequent plots are created from data taken after the array had been exposed to a total dose of $8.33 \times 10^7/\text{cm}^2$ (2 months equivalent). Again, the total dosage here was equal to 2 months, but the period between the first annealing and this one was equivalent to 1 month.

Figure 2 shows the dark density distribution of one of the 1.5 hr dark exposures over plotted with the density distributions of the three populations of hot pixels. Note that most of the signal in this dark exposure is below

Table 1. Number of hot pixels and their annealing rates

Fluence/WFC3 Orbit Equivalent	>40 e^-/px/hr	>80 e^-/px/hr	>160 e^-/px/hr
After 8.33×10^7/1 month*	<57670	<29217	<15310
1 month annealed	4724	1397	415
1 month annealing rate	<91.8%*	<95.2%	<97.3%*
After 1.67×10^8/2 months	28421	19417	12275
2 months annealed	9479	2816	813
2 months annealing rate	66.6%	85.5%	93.4%
After 2.50×10^8/3 months	31046	19629	12297
3 months annealed	9972	2784	920
3 months annealing rate	67.9%	85.8%	92.5%
After 2.50×10^9/2.5 years	553837	412937	268129
2.5 years annealed	106465	33731	10210
2.5 years annealing rate	80.8%	91.8%	96.2%

*1 month data contaminated when ^{55}Fe slipped down to expose device.

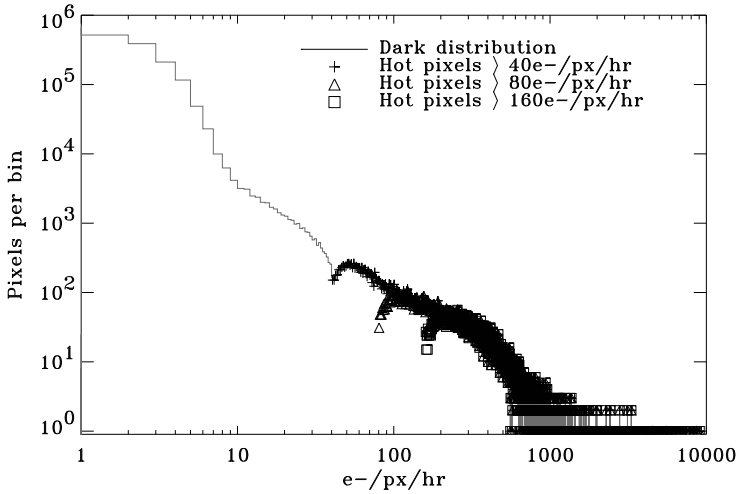

Figure 2. This figure shows the dark signal distribution, over plotted with the the distribution of the hot pixel populations, immediately after irradiation, at -83°C.

10 e^-/px/hr (the mean dark is on the order of 0.4 e^-/px/hr). The shape of the main peak is determined by read noise (3 e^- rms) while the tail is dominated by hot pixels. The dip observed in the main distribution at 40 e^-/px/hr is an artifact of the identification and removal of the random events. There is an uncertainty in the identification of these events which is equal to the shot noise of the signal; signals near the threshold may be above or below the threshold. This is more thoroughly discussed in the first paper.[5] This same effect can be seen in the distribution of hot pixels where a dip is observed at each threshold.

The subsequent data was plotted in a similar manner, with the dark signal distributions at each temperature over plotted with the distribution of the hot pixels at that same temperature. Note that these distributions do not contain the saturated pixels.

The annealing process starts at -40°C, a much cooler temperature than expected based on the experiences of the HST Space Telescope Imaging Spectrograph.[8] Figure 3 shows that a significant portion of the hot pixels have begun to move toward the main population.

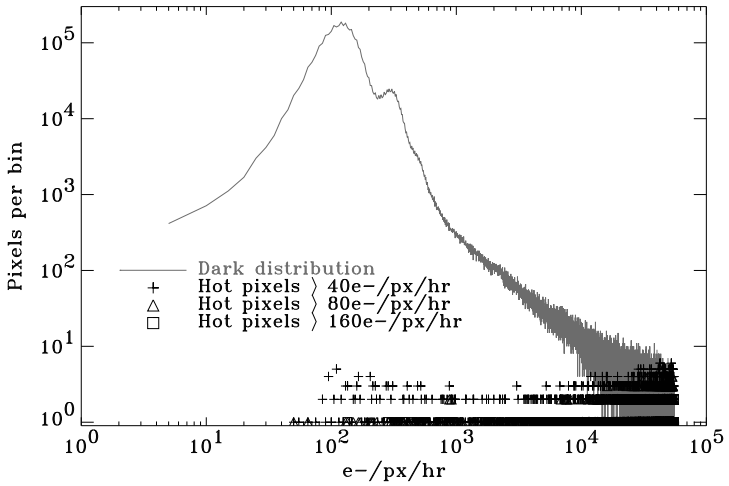

Figure 3. This figure shows the dark signal distribution, over plotted with the distribution of the hot pixel populations, at -40°C.

As the CCD warms the number of annealed pixels increases (figure 4), and hot pixel annealing continues to be observed as the temperature increases. However, as the temperature increases the dark population is pushed out of the available dynamic range. Figure 5 shows that at +10°C the mean dark moves closer to the high end of the dynamic range and hot pixels are mostly saturated. This becomes even more severe as the temperature increases (figure 6) and at these temperature ranges the tendency for hot pixels to anneal is masked by the reduction of dynamic range and consequent saturation. What is noted, though, is that the majority of the hot pixels that are not saturated never fully rejoin the main population. While they have fallen below the threshold that defined them as hot pixels, their dark signal is still higher than most of the other pixels (see figures 5, and 6).

Figure 7(a) is a reminder of the dark distribution before annealing, as the CCD is warming up, at -40°C. Figure 7(b) is the dark distribution after the CCD has annealed and is cooling down, at -40°C. These are shown together so that the shape of the two distributions can be compared side by side. Note that figure 7(b) illustrates what portion of the fully annealed hot pixel population is available for analysis at this temperature. Comparison between figures 7(a) and 7(b) helps to appreciate the level of annealing at -40°C. As mentioned earlier, a quantitative comparison is difficult since the mean dark at -40°C after annealing is approximately 3 times lower than that before annealing.

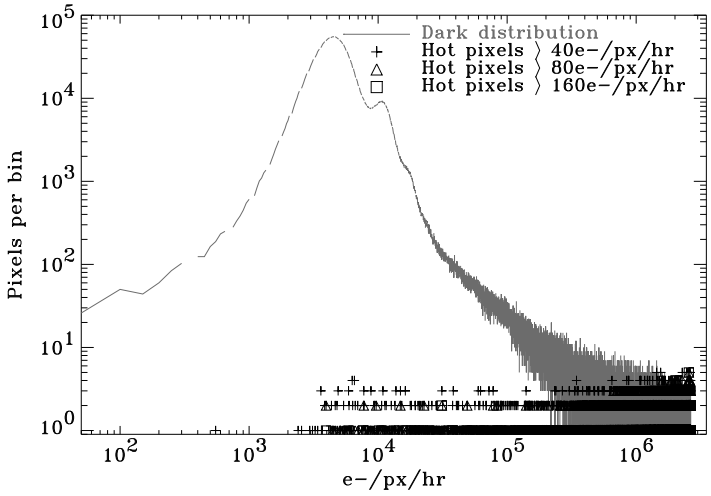

Figure 4. This figure shows the dark signal distribution, over plotted with the distribution of the hot pixel populations, at -10°C.

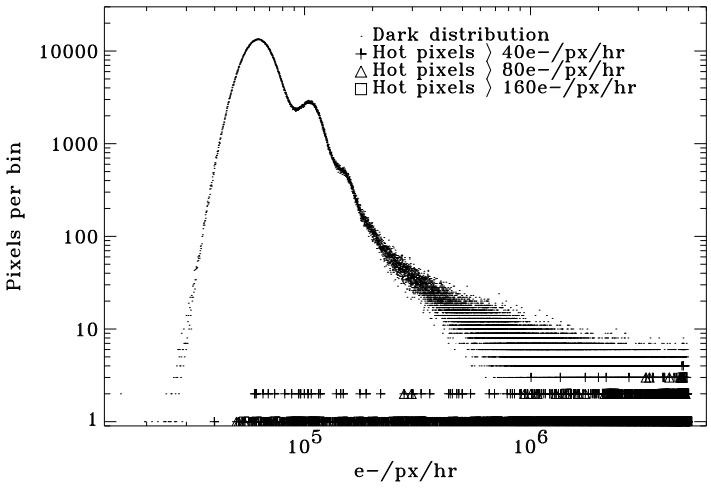

Figure 5. This figure shows the dark signal distribution, over plotted with the distributions of the hot pixel populations, at +10°C.

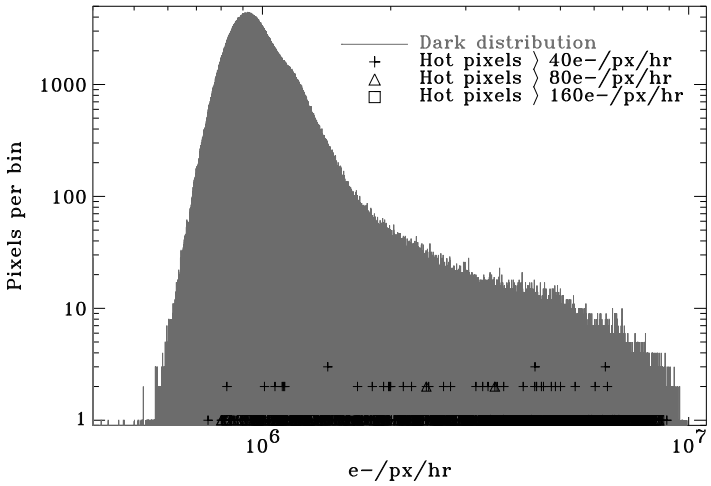

Figure 6. This figure shows the dark signal distribution, over plotted with the distributions of the hot pixel populations, at +30°C.

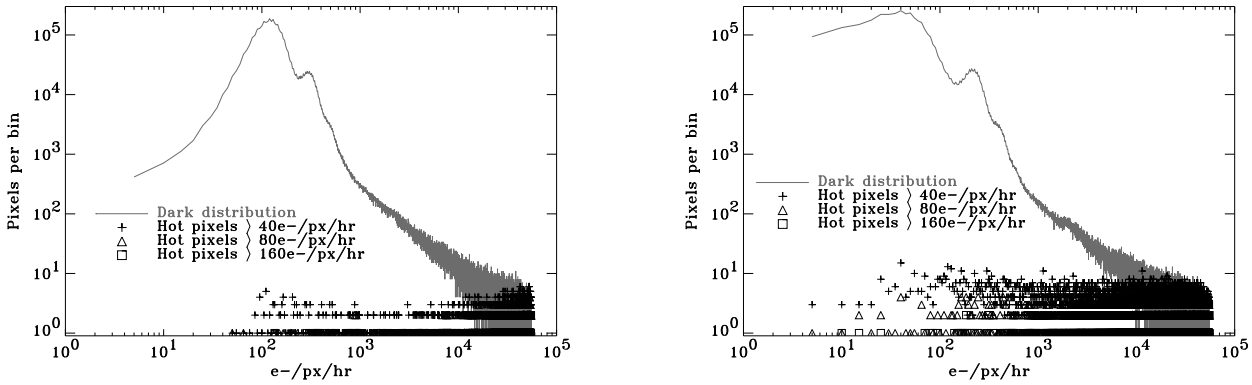

Figure 7. Side a is a repeat of figure 3, the dark signal distribution, over plotted with the distributions of the hot pixel populations before annealing, at -40°C, for side by side comparison. Side b is the dark signal distribution, over plotted with the distributions of the hot pixel populations, after annealing, at -40°C.

Figure 8(a) is a reminder of the dark signal distribution at -83°C before annealing so that the shape of the distributions can be compared. Figure 8(b) shows the dark distribution after the CCD has returned to -83°C, as well as the hot pixel distribution. Most of the hot pixels have annealed (>90% of the >160 e^-/px/hr hot

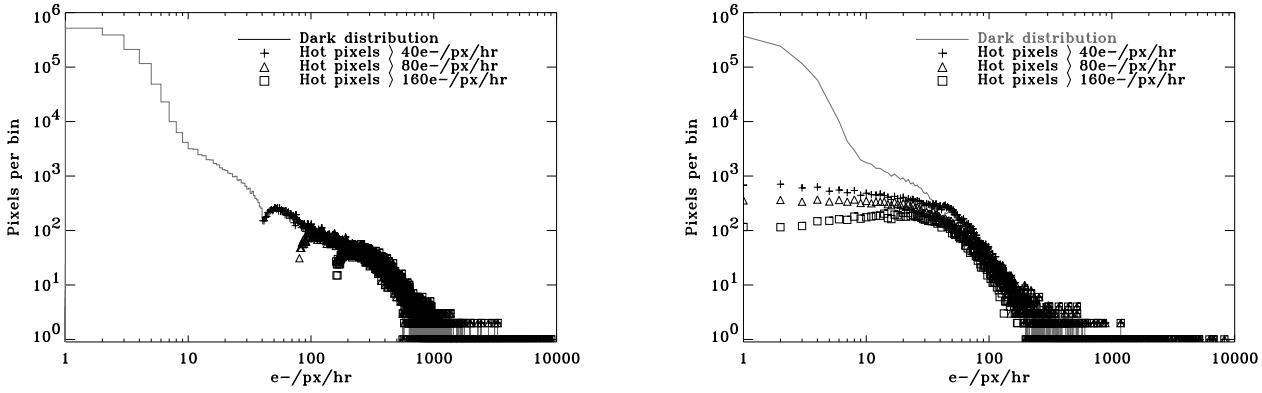

Figure 8. Side a is a repeat of figure 2: the dark signal distribution, over plotted with the distributions of the hot pixel populations, immediately after irradiation, at -83°C, for side by side comparison. Side b is the dark signal distribution, over plotted with the distributions of the hot pixel populations, after annealing, at -83°C.

pixels), but there are still a significant number evident in the tail of the histogram.

Figure 9 shows the dark signal distribution plot of the entire array at -83°C, for both before and after annealing. Note the difference in the width of the histograms and the shape of the tails.

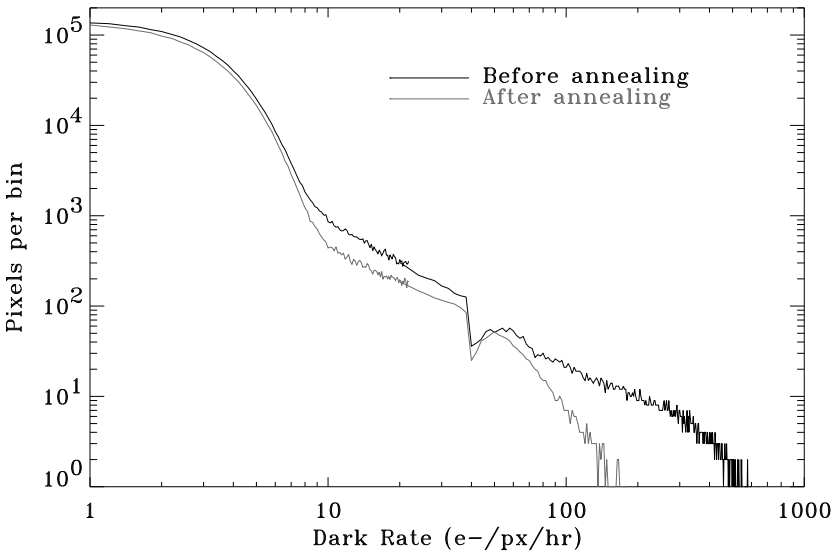

Figure 9. This figure shows the dark signal distribution at -83°C, both before and after annealing.

Figure 10 shows the number of hot pixels that annealed and whose magnitude had fallen below 100x and 200x the mean of the dark distribution. The annealing process starts somewhere around -40°C, really ramps up

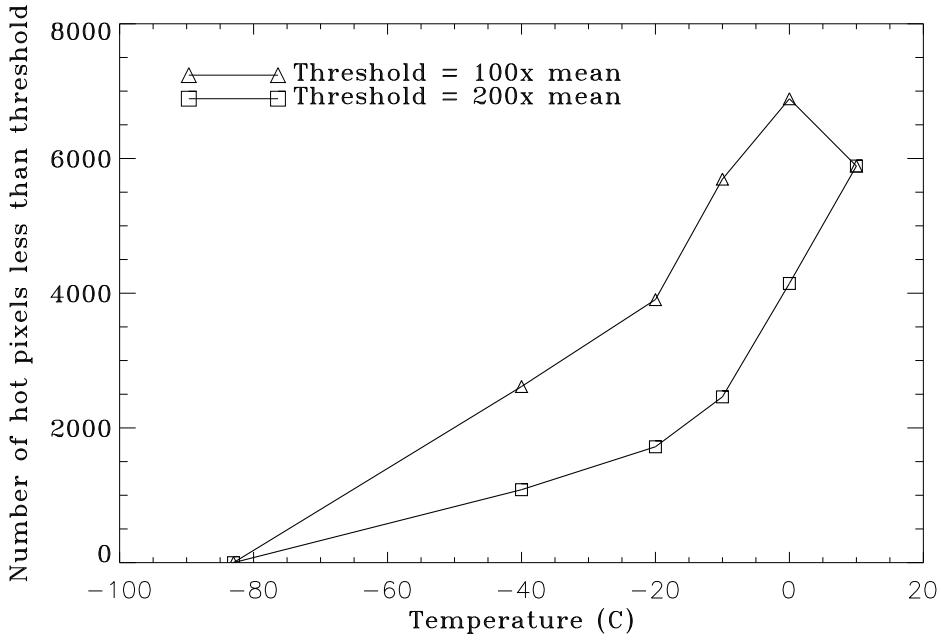

Figure 10. The number of annealed hot pixels vs. temperature shows more clearly that annealing begins at -40°C.

between -20°C and -10°C, and continues through warmer temperatures. The peak in the number of annealed pixels at 0°C and the following decay for the 100x mean dark threshold are artifacts caused by the saturation of hot pixels. Above this temperature the thresholds (of 100x and 200x mean dark current) are higher than the available dynamic range and the number of non-saturated hot pixels rapidly decreases.

5. CONCLUSION

The results of the experiment demonstrated that hot pixel annealing starts at temperatures as low as -40°C. The probability of a hot pixel being annealed depends on its initial dark signal: hotter pixels are more likely to anneal than warm pixels. The annealing process does not fully return the hot pixel to its original state: its dark current tends to be higher than average. Radiation damage increases the mean value of the dark current, and the subsequent anneal significantly reduces the increase in the mean value of dark signal.

ACKNOWLEDGMENTS

This work was funded by the Wide Field Camera 3 project. We would like to thank the NASA Electronics and Packaging Program (NEPP) for their generous support.

REFERENCES

1. R. A. Kimble, P. Goudfrooij, and R. L. Gilliland, "Radiation damage effects on the CCD detector of the Space Telescope Imaging Spectrograph," in *UV, Optical and IR Space Telescopes and Instruments*, J. B. Breckinridge and P. Jakobsen, eds., *Proc. SPIE* **4013**, pp. 532–544, 2000.
2. M. Sirianni, M. Clampin, G. Hartig, H. Ford, G. Illingworth, V. Argabright, B. Burmester, G. DeMarchi, W. Koldewyn, A. Martel, M. Mutchler, A. Riess, R. Schrein, and P. Sullivan, "Characterization and on-orbit performance of the Advanced Camera for Surveys CCDs," in *Future EUV/UV and Visible Space Astrophysics Missions and Instrumentation*, J. C. Blades and O. Siegmund, eds., *Proc. SPIE* **4854**, pp. 496–506, 2003.

3. A. Waczynski, E. J. Polidan, P. W. Marshall, R. A. Reed, S. D. Johnson, R. J. Hill, G. S. Delo, E. J. Wassell, and E. S. Cheng, "A comparison of charge transfer efficiency measurement techniques on proton damaged n-channel CCDs for the Hubble Space Telescope Wide-Field Camera 3," *IEEE Transactions on Nuclear Science* **48**, pp. 1807–1814, 2001.
4. S. D. Johnson, A. Waczynski, P. Marshall, E. Polidan, and R. A. Reed, "An analysis of charge transfer efficiency noise on proton-damaged CCDs for the hubble space telescope wide field camera 3," in *Photonics for space environment VIII*, E. Taylor, ed., *Proc. SPIE* **4823**, pp. 245–253, 2002.
5. E. Polidan, A. Waczynski, P. Marshall, S. D. Johnson, C. Marshall, R. Reed, R. A. Kimble, G. Delo, D. Schlossberg, A. M. Russell, T. Beck, Y. Wen, J. Yagelowich, R. J. Hill, and E. Wassell, "Hot pixel behavior in WFC3 CCD detectors irradiated under operational conditions," in *Focal Plane Arrays for Space Telescopes*, T. J. Grycewicz and C. R. McCreight, eds., *Proc. SPIE* **5167**, pp. 258–269, 2003.
6. C. J. Dale, P. W. Marshall, B. Cummings, L. Shamey, and A. Delamere, "Spacecraft displacement damage dose calculations for shielded CCDs," *Proc. SPIE* **1656**, pp. 476–487, 1992.
7. G. R. Hopkinson, C. J. Dale, and P. W. Marshal, "Proton effects in CCDs," *IEEE Transactions on Nuclear Science* **43(2)**, pp. 614–627, 1996.
8. R. Kimble, *private communication*, 2003.